THE BELL SYSTEM
TECHNICAL JOURNAL

Volume 47 November 1968 Number 9

Influence of Bulk and Surface Properties on Image Sensing Silicon Diode Arrays

By T. M. BUCK, H. C. CASEY, Jr., J. V. DALTON, and M. YAMIN

(Manuscript received March 7, 1968)

Silicon diode arrays for use as the electron-beam accessed target in camera tubes for the **Picturephone**® *visual telephone set have been fabricated and their properties evaluated. These targets offer significant advantages over the antimony trisulfide target commonly used in vidicon-type tubes. But there are certain potential limitations which must be dealt with in developing a silicon target. Three of its critical requirements are adequate sensitivity to visible light, low dark current, and junction uniformity and freedom from defects across at least 300,000 diodes per square centimeter. Sensitivity to visible light is expressed here by the efficiency for conversion of incident photons to electrons in the read-out circuit. Conversion efficiencies exceeding 50 percent in the visible region have been achieved by oxidizing or by diffusing phosphorus into the light-receiving surface to reduce the surface-recombination velocity. Diode leakage currents of* $\leqq 1 \times 10^{-13}$ *A per diode are required, and are obtained for target voltages up to about 5 to 7 V. Surface generated current dominates in the 8-*μ *diameter diodes of the array, but this component of current can be reduced substantially by use of (100) surfaces or by hydrogen annealing. Visible defects in a picture can result from leaky diodes or oxide pinholes which cause bright spots, and diodes covered by oxide which cause dark spots. Our best targets show a video display with only a few defects; processing must be improved to eliminate defects completely.*

I. INTRODUCTION

A television camera tube with a silicon diode array target has been reported recently by Crowell, Gordon and their co-workers.[1-3] A target of the general type used in this tube was first proposed in 1951 by Reynolds,[4] later discussed by Heijne,[5] and recently analyzed by Wendland.[6] It is similar, but not identical in operation, to the evaporated-film photoconductive target, typically antimony trisulfide, which is commonly used in vidicon TV camera tubes.[7]

A vidicon-type tube is of interest for use in the *Picturephone*® visual telephone station set because it is the least expensive and smallest camera tube that has the required sensitivity and resolution. The silicon target has certain potential advantages over the evaporated-film photoconductive target.

This paper describes the effect of bulk and surface properties on the performance of the silicon target. The properties that dominate the conversion of incident photons to electrons in the external circuit and the diode leakage current are analyzed in detail. These analyses, together with the relevant processing techniques and resulting behavior, have been combined into a description of silicon diode arrays for image sensing.

The operation of the silicon target is illustrated in Fig. 1. A scanning electron beam charges the diode-array side of the silicon target down to cathode (ground) potential while the n-region is held a few volts above ground. This puts reverse bias on the diodes. Light shining on the other side of the target and absorbed in the n-region generates holes, some of which diffuse to the diodes and reduce the negative charge on the p-regions. This reduction establishes a stored charge pattern. The scanning electron beam returning to the site of the diode deposits more negative charge, an amount proportional to the light intensity. The recharging current constitutes the video signal. Leakage of the charge pattern established by the light is prevented by the rectifying p-n junction rather than by high bulk resistivity as in the case of antimony trisulfide. The usual time between scans of the electron beam at a given diode site is 1/30 second.

The silicon target has several advantages over evaporated-film photoconductive targets such as antimony trisulfide:

(*i*) It does not show aging effects (burn-in) by intense light to which it might be exposed accidentally, or by the electron beam. The absence of burn-in by the electron beam permits electronic zooming.

(*ii*) Its photoconductive lag is negligible.

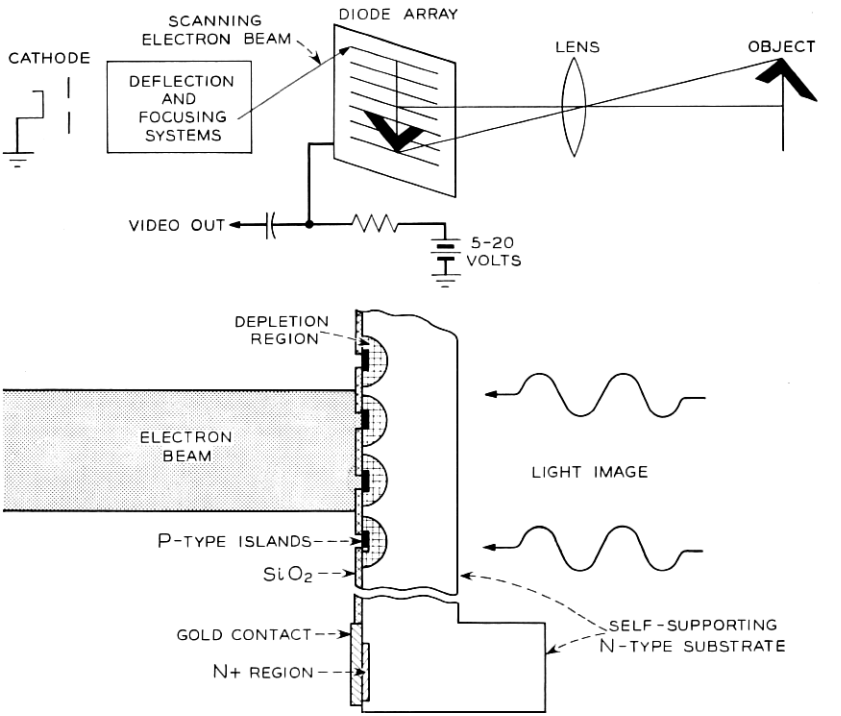

Fig. 1 — Schematic diagrams of silicon target, illustrating principle of operation.

(*iii*) It does not deteriorate on heating to temperatures sufficiently high (≈350°C) for good tube processing required for long life.

There are, however, certain potential problems and limitations which must be considered in developing a successful silicon diode array target for a camera tube. Three of these, related to materials and process factors, are:

(*i*) The target must have adequate sensitivity to visible light. We express sensitivity as conversion efficiency η_c which is defined as the ratio of electrons that flow in the external circuit to the number of incident photons. For photons in the 0.45 to 0.8-μ wavelength range, a value of $\eta_c > 20$ percent would be satisfactory.

(*ii*) The total dark current should be less than 50×10^{-9} A, which means diode leakage current for each of the approximately 1/2 million diodes must be $\leqq 1 \times 10^{-13}$ A, so that only a negligible amount of charge will leak off between scans of the electron beam. For camera

tube applications total diode capacitance is restricted to a rather narrow range. Preliminary results indicate that a substrate resistivity of 10 ohm-cm, which yields 2000 pF/cm^2 at 10 V reverse bias, is close to the optimum.[2]

(*iii*) The whole array must have uniform properties and be free of defects which can cause bright spots or dark spots in the display-tube picture.

Tube performance is, of course, the ultimate test of a good target, but for studies of efficiency and diode leakage it was convenient to make measurements outside the tube. We demonstrate the relationship between these measurements and the actual tube performance.

II. TARGET STRUCTURE

The target, as illustrated in Fig. 2, is a thin disk of n-type silicon with an array of p-n diodes on one side. These are the sensing ele-

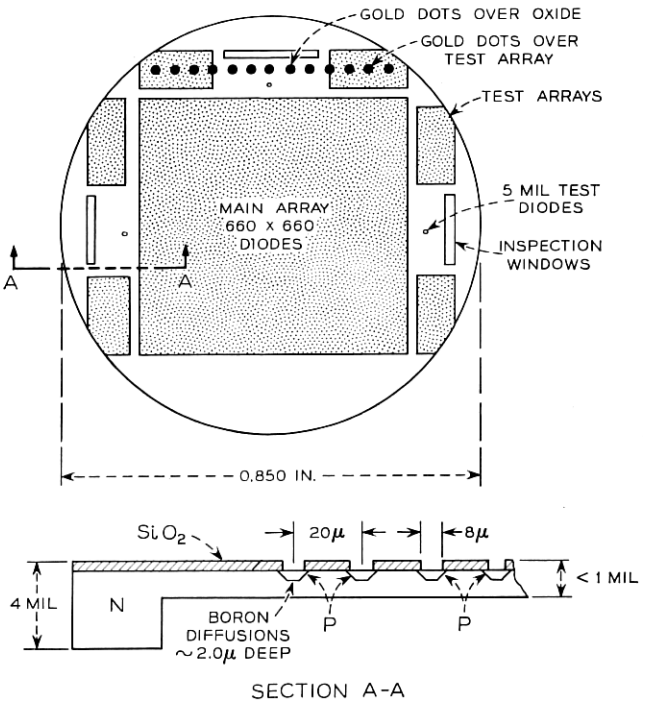

Fig 2 — Details of target structure (660 × 660 array).

ments. Silicon dioxide covers the n-type silicon between the diodes to keep the electron beam from landing there. The oxide also protects the junction edges and reduces surface leakage. In a typical design the target is 0.850 inch in diameter, 0.5 to 1 mil thick in the light sensing region, and has a 4-mil-thick rim for support. The diodes are 8 μ in diameter and are on 20 μ centers in an array of 660 $\times$ 660.

Outside the main array are 5 mil p-n diodes which can be probed for measurements at various stages of processing. There are also gold dots over the oxide for MOS measurements and gold dots over test arrays of 8 μ diodes for reverse current measurements which simulate dark current measurements in the tube. Ohmic contact to the n-region is made through an annular n^+ region which is in the thick ring on the light-receiving side of the target. The dimensions just given are representative of many targets which have been made, although larger and denser arrays are also being studied.

Planar technology is used in the fabrication with the following deviations from typical device processing:

(*i*) One-step diffusions are used, with no drive-in.

(*ii*) There is no postdiffusion reoxidation and therefore no second photoresist step or reregistration.

(*iii*) The phosphorus diffusion for ohmic contact is the last high temperature step, for reasons discussed near the end of Section 3.3.

An additional processing step, the deposition of a semi-insulating film over the diode side, is usually performed before the target is mounted in a tube. The purpose of this film is to dissipate charge, deposited by the electron beam, from the target area between the diodes. Several films have been developed for this purpose by Crowell and Labuda.[2] Targets described in this paper did not have such films except in cases where tube measurements are mentioned.

III. CONVERSION EFFICIENCY

3.1 *Calculation of Conversion Efficiency*

If a silicon diode array target is to replace the antimony trisulfide target in a vidicon-type camera tube, its sensitivity should approximate or exceed that of antimony trisulfide targets. We describe sensitivity in terms of the conversion efficiency η_c which is defined as the ratio of the number of electrons that flow in the external circuit to

the number of incident photons. Efficiency of antimony trisulfide targets is typically 20 percent at 5500 Å and falls off toward both ends of the visible region. For silicon targets the conversion efficiency will depend on the sample thickness, the wavelength of the light and several properties of the semiconductor. In order to identify the important parameters and their effects on the conversion efficiency, the steady-state, short-circuit current in a one-dimensional model of a single p-n junction has been calculated.

The most important relation governing distribution of the optically generated carriers in the semiconductor is the continuity equation. The continuity equation formulation for the transport of carriers has been rigorously treated by van Roosbroeck.[8] From that treatment the steady-state, small-signal differential equation for the minority carrier density in excess of the equilibrium concentration at zero total current and electric field in the one dimension x is

$$D_p \frac{d^2p(x)}{dx^2} - \frac{p(x)}{\tau_p} = -G(x), \tag{1}$$

where $p(x)$ is the excess minority carrier density, D_p the hole diffusion coefficient, τ_p the hole lifetime, and $G(x)$ the net carrier generation rate.

At one boundary, the surface at $x = 0$, the hole flux as determined by the surface-recombination velocity S must equal the diffusive flux:

$$j(0) = qSp(0) = q\, D_p \frac{dp}{dx}\bigg|_{x=0}. \tag{2}$$

The other boundary condition refers to the edge of the junction space-charge region located at depth $x = d$ from the illuminated surface. For the short-circuit condition, the excess hole density at the junction edge is zero,

$$p(d) = 0, \tag{3}$$

and the short-circuit current density i_{sc} is

$$i_{sc} = -q\, D_p \frac{dp}{dx}\bigg|_{x=d}. \tag{4}$$

When the generation rate for carriers is governed by Lambert's law of photon absorption, the net generation rate may be written as

$$G(x) = \frac{(1 - R)N}{A}\, \alpha \exp(-\alpha x), \tag{5}$$

where R is the reflectivity, N the number of incident photons per unit time, A the cross-sectional area, and α the optical absorption coefficient. The conversion efficiency, neglecting absorption in the junction space-charge region, becomes

$$\eta_c = \frac{i_{sc/q}}{N/A} = \frac{-D_p \left.\frac{dp}{dx}\right|_{x=d}}{N/A}. \tag{6}$$

The conversion efficiency may be obtained from equation (1) with the conditions expressed by equations (2) through (5) and the definition of equation (6). Since the generation rate $G(x)$ has a dependence on wavelength through both the reflectivity and absorption coefficient, η_c will depend on wavelength. As Section 3.3 describes in detail, difficulty has been encountered in reconciling the experimental and calculated η_c for illuminated surfaces that have been etched and aged in air. The experimental η_c for the etched surface is always significantly less than the calculated η_c, even with very high S, when a significant portion of the carriers are generated near the illuminated surface.

This situation is similar to Wittry and Kyser's[9, 10] experiences with cathodoluminescence in GaAs. Their cathodoluminescence intensity was less than could be explained by a high surface recombination alone. They assumed that minority carriers generated between the surface and a depth δ are not effective in producing recombination radiation. Similarly, in the present work it was found necessary to modify the generation rate given by equation (5) to account for a "dead layer" at the surface in order to obtain agreement between the calculated and experimental η_c.

The effect of a "dead layer" on the conversion efficiency has been introduced into the analysis by assuming that the carriers generated within a distance δ of the illuminated surface cannot diffuse to the junction and be collected. For a solid in which all the incident photons, less those lost by reflection, are absorbed in creating hole-electron pairs, the number of carriers per unit area generated between the surface and $x = \delta$ is found by integrating $G(x)dx$ between the limits 0 and δ. Thus, there will be $(1-R)N[1 - \exp(-\alpha\delta)]$ carriers generated within a distance δ of the surface. The number of holes that may be collected in the absence of a "dead layer" or surface and bulk recombination is equal to the number of absorbed photons and is simply $(1-R)N$. If the carriers generated between $x = 0$

and δ are lost and not available for collection, then the carriers available for collection in the absence of other losses is simply the difference of these two quantities, $(1-R)N \exp(-\alpha\delta)$. Therefore, a generation rate of

$$G'(x) = \left[\frac{(1-R)N}{A}\,\alpha \exp(-\alpha x)\right] \exp(-\alpha\delta), \tag{7}$$

when integrated from 0 to ∞, will give the same number of collectable carriers as $[(1-R)N/A]\ \alpha \exp(-\alpha x)$ integrated from δ to ∞: that is,

$$\int_0^\infty G'(x)\,dx = \int_\delta^\infty G(x)\,dx.$$

This formalism, which has been found useful in representing the effect of the surface space-charge region on optically generated carriers, permits retaining the field-free continuity equation and the representation of surface recombination by S. The conversion efficiency for the generation rate given by equation (7) is

$$\eta_c = \frac{\exp(-\alpha\delta)(1-R)\alpha L_p}{\alpha^2 L_p^2 - 1}\left\{\left[\frac{(S + \alpha L_p^2/\tau_p)\ \mathrm{sech}\ (d/L_p)}{(S \tanh (d/L_p) + L_p/\tau_p)}\right] - \left[\alpha L_p + \tanh (d/L_p) + \frac{S\ \mathrm{sech}^2\ (d/L_p)}{(S \tanh (d/L_p) + L_p/\tau_p)}\right] \exp(-\alpha d)\right\}, \tag{8}$$

where the minority carrier diffusion length L_p is given by $L_p = (D_p\tau_p)^{1/2}$. The efficiency η_c will be expressed in percent. To further describe the "dead layer" and delineate the role of bulk and surface recombination on the target sensitivity, it is necessary to compare the experimental η_c variation as a function of wavelength with η_c calculated from equation (8).

3.2 *Experimental Procedure for Efficiency Measurements*

To evaluate the properties of the silicon diode arrays, it was convenient to make measurements outside the tube. Targets for this purpose had large diodes and had received the same processing as the 8-μ diode arrays except that the semi-insulating film was omitted. Figure 3 illustrates the structure used. The pattern with diodes from 5 to 40 mils in diameter was used so that the effect of diode diameter on η_c for a given light-spot size could be determined. Because equation (1) applies only to a one-dimensional problem, one-dimensional experimental conditions must be achieved. These conditions were

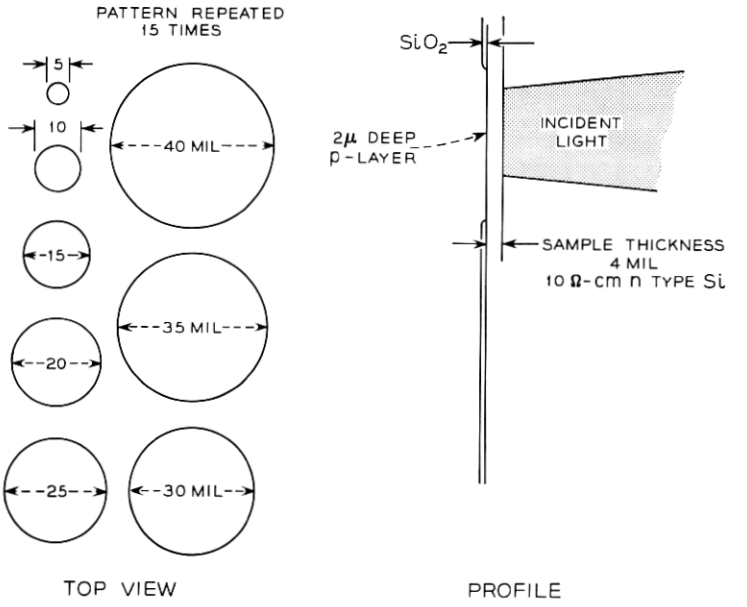

Fig. 3 — Array of large diodes for studies of conversion efficiency and diode leakage.

taken to apply whenever further increase in diode diameter did not increase the conversion efficiency, which occurred for diameters greater than 30 mils. The η_c measurements reported here were taken with the 40-mil diameter diodes.

The experimental arrangement for measuring the conversion efficiency is illustrated in Fig. 4. Emission from the tungsten 250 W quartz-iodine lamp was filtered by a Corning filter C. S. 1-69 (heat-absorbing glass) to reduce the infrared intensity. Plane mirror M_1 and spherical mirror M_2 focused the light onto the entrance slit of the Perkin–Elmer model 99 single-prism spectrometer. The light was chopped at the spectrometer entrance at 37.5 Hz. An Optics Technology band-pass filter was used at each measurement wavelength to prevent light of undesired wavelengths from being transmitted through the spectrometer. The light from the spectrometer exit slit could be directed to the sample or to a calibrated thermocouple by the movable mirror. The spherical mirror M_3 focused the radiation onto the thermocouple whose output was measured with the Princeton Applied Research model HR-8 lock-in amplifier.

The spot size of approximately 4 × 12 mils on the sample was obtained

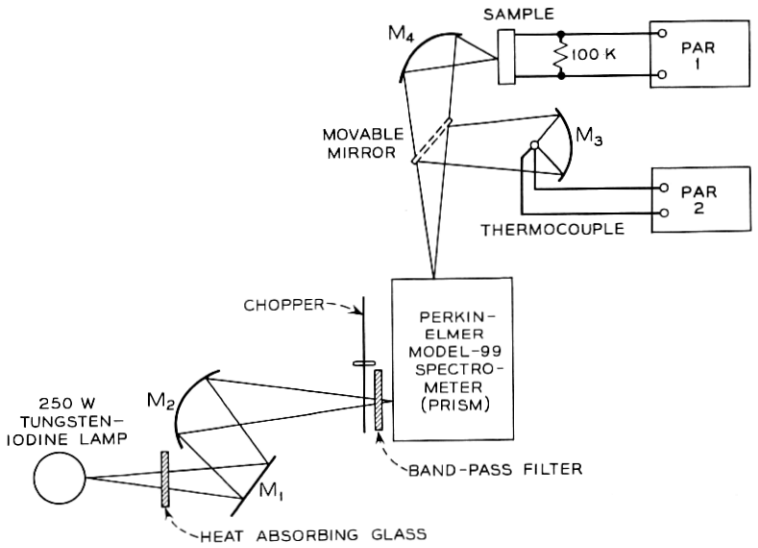

Fig. 4 — Experimental arrangement for measurements of conversion efficiency.

by reducing the height of the spectrometer slits and using M_4, a 90° ellipsoidal mirror with a 6 : 1 reduction. The short-circuit current was determined by measuring the voltage across a 100 KΩ resistor connected between the n and p sides of the diode. To maintain junction short-circuit conditions, the light intensity was kept low enough so that the junction voltage was $\leqq 0.1\ kT/q (\leqq 0.002$ V). Linearity with light intensity was confirmed with neutral density filters and absence of significant leakage currents could be demonstrated by linear variation of junction voltage with load resistance.

In order to make quantitative comparison of the experimental and calculated η_c the absolute photon flux must be known. For this purpose, a silicon solar cell was calibrated by comparison with several calibrated thermopiles. Then the calibrated solar cell was placed in the position of the sample and the spectrometer thermocouple was calibrated. The absolute photon flux can be assigned an uncertainty of ±10 percent.

3.3 *Experimental and Calculated Conversion Efficiency*

In this section the control of target efficiency by process variations is discussed. Experimental efficiency data are compared with calculated curves, and this permits determination of the parameters L_p, S, and δ. Consideration of equation (8) shows that the best discrimination between L_p, S, and δ is obtained when d is two to four times L_p.

Preliminary measurements indicated that a 4-mil target thickness was suitable. The wavelength dependence of the absorption coefficient α was taken from the data of Dash and Newman,[11] and the reflectivity R for an etched silicon surface was taken from Philipp and Taft's data.[12] The hole diffusion coefficient D_p was assigned a value of 10 cm^2 per second. Given these experimental dependences of α and R, the wavelength becomes the independent variable for equation (8), and the variation of η_c with wavelength is determined by the physical parameters d, L_p, S, and δ.

Initially, consider the data in Fig. 5 for the etched surface aged in air (the dots). The calculated η_c curve for a generation rate expressed by equation (5) (no "dead layer") is shown by the dashed line. The diffusion length L_p has been assigned a value of 50 μ to produce agreement between the calculated and experimental η_c in the long wavelength region. The use of the generation rate of equation (5) is equivalent to $\delta = 0$ in equation (8) for η_c. Even with the maximum value of surface-recombination velocity $S_{max} = (kT/2\pi m)^{\frac{1}{2}} \approx 10^7$ cm per second, the calculated η_c does not decrease as rapidly at short wavelengths as the experimental η_c. The discrepancy between the calculated and experimental η_c for wavelengths in the visible region leads to the "dead layer" concept.

Fitting the data in Fig. 5 with a finite δ in equation (8) does not lead to unique values of S and δ. However, their values are limited to a reasonably narrow range. For example, by plotting the experimental data with the calculated η_c (lower curve, Fig. 5) it is not possible to discriminate between values of $S = 10^7$ cm per second, $\delta = 0.8$ μ, and $S = 6 \times 10^4$ cm per second, $\delta = 1.8$ μ. The larger δ value was obtained with a nonlinear least-squares technique described by Marquardt.[13] The high surface-recombination velocity agrees with earlier studies of Buck and McKim[14] and Harten[15] in which it was shown that S is normally very high on an etched silicon surface. Harten's[15] measurement technique was similar to the one described here. To resolve this ambiguity in S and δ, experimental data at wavelengths less than 0.45 μ are necessary. Because the efficiency of the diode is rapidly decreasing and the intensity of the light source is also becoming smaller, measurements in this wavelength range are not presently possible. The significant point is that the "dead layer" thickness is approximately a micron and S is very high.

In order to gain insight into the significance of the "dead layer," the surface potential was determined by surface conductivity meas-

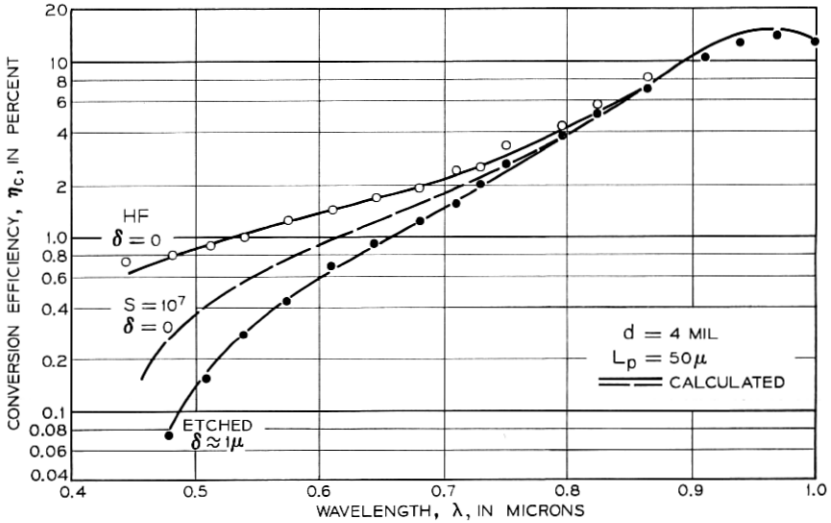

Fig. 5 — Conversion efficiency as function of wavelength for etched and HF-treated surfaces. Target is 4 mils thick.

urements[14] on silicon slices from the same 10 ohm-cm n-type crystal. The surface was found to be in a condition of depletion with the potential varying from −0.25 V at about ½ h after etching to −0.6 V (energy bands bent upward) after several hours of aging in air. The variation of potential within the surface depletion region was obtained from Poisson's equation[16] for a donor concentration of 6.0×10^{14} cm^{-3}. Because the electric field in the surface depletion region goes to zero very slowly it is difficult to define a depletion-region depth. If, however, the potential from Poisson's equation is approximated by a simple parabolic potential of the form

$$V(x) = (V_s/x_s^2)(x - x_s)^2, \tag{9}$$

where V_s is the surface potential, then the depletion layer thickness may be approximated by x_s. The quantity x_s is determined by a reasonable fit from $x \cong 0.1x_s$ to $x \cong 0.8x_s$. For a surface potential of −0.25 V, x_s is 0.8 μ and for −0.60 V, x_s is about 1.1 μ. Therefore, the depletion layer thickness is about the same as the "dead layer."

Because the depth of the "dead layer" and the surface depletion region are about the same, it is reasonable to attribute the "dead layer" to the surface depletion region. This assumption suggests that

the "dead layer" results from the built-in field at the surface whose direction is such as to oppose the diffusion of holes to the junction. To test this hypothesis, reversal of the surface field should eliminate the "dead layer" because the field for holes would be in the same direction as the diffusion toward the junction. It has been shown[14, 15] that a hydrofluoric acid treatment bends the energy bands downward at a silicon surface temporarily. In the present work a surface potential of +0.2 V was determined after such treatment. The upper curve in Fig. 5 shows that the experimental data for an HF-treated surface may be fitted with the same L_p, but no "dead layer" is required. Aging in air causes a shift in surface potential back to a depletion condition and a response that requires a "dead layer" correction.

Although a 4-mil target thickness is useful in efficiency studies for discriminating among the critical parameters, a target for a camera tube should be $\leqq 1$ mil thick for adequate resolution. For a 1 mil thickness Fig. 6 shows two sets of experimental data together with calculated curves which illustrate the importance of S and δ. Consider first the experimental data for the etched surface (the dots). The L_p of 32 μ was obtained from the η_c measurement at a thickness of 4 mils before

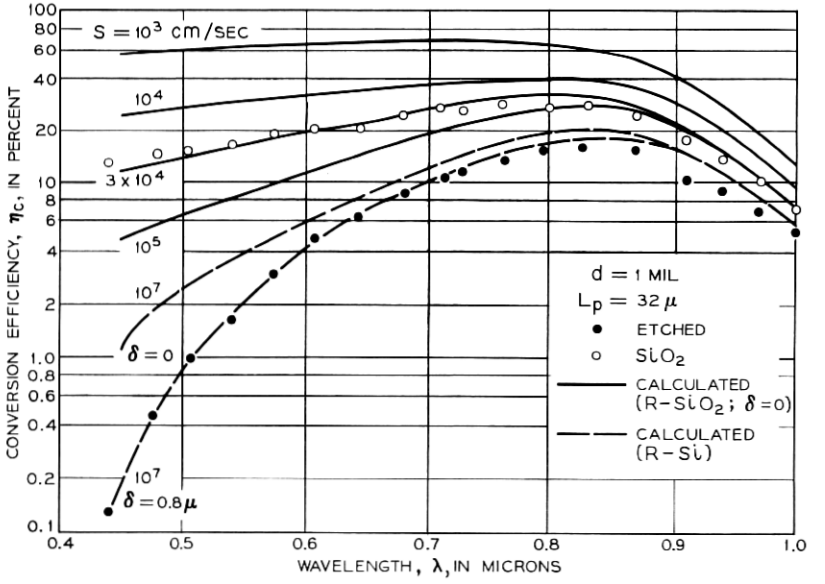

Fig. 6 — Influence of surface-recombination velocity on efficiency for 1-mil thick target.

the target was thinned to 1 mil. The values of $S = 10^7$ cm per second and $\delta = 0.8\ \mu$ were previously shown to be representative of an etched surface.

The dashed lines are calculated for $S = 10^7$ cm per second and $\delta = 0$ or $0.8\ \mu$ to illustrate the effect of the "dead layer" at this thickness. It may be seen that the efficiency in the visible region drops from 10 percent at $0.7\ \mu$ to 1 percent for high S and no "dead layer," but drops to 0.1 percent for the $0.8\ \mu$ "dead layer." Calculations based on equation (8) show that when $d \leqq L_p$, further increase in L_p does not improve efficiency very much. This also means that efficiency is insensitive to small lateral variations in d which may occur during etching. However, S and δ have a strong influence on efficiency and these parameters must be substantially decreased. The HF treatment and other chemical treatments[14,15] on the etched surface which reduce S and δ are too unstable for long life in a camera tube.

A more permanent improvement in efficiency can be made by high temperature oxidation of the surface. Experimental efficiency data taken after a light steam oxidation (900°C for 10 minutes) are also shown in Fig. 6 (circles). Oxidation raised efficiency above 10 percent at the blue end of the visible region. Values of $S = 3 \times 10^4$ cm per second and $\delta = 0$ yield a calculated efficiency curve which fits the experimental points. Values of S for steam oxide with no further treatment have been as low as 10^3 cm per second which gives an efficiency of 50 to 60 percent. The 800 Å oxide also serves as an antireflection coating which contributes an additional slight increase in efficiency.

Experimentally determined reflectivity of the oxidized surface was used in equation (8) to obtain the solid curves shown in Fig. 6. No "dead layer" correction was needed for the oxidized surface. This is attributed to the fact that the oxidized surface is more n-type than the bulk; the energy bands are bent downward at the surface, eliminating the depletion layer. The HF soak eliminated the "dead layer" temporarily for the same reason, that is, it bends the bands down at the surface.

It is assumed that oxidation reduces S both by reducing the density of recombination centers and by shifting surface potential, although the data to confirm this are not complete. Surface potential is shifted from about -0.6 V, the previously mentioned depletion-layer condition for an etched surface, to $+0.2$ V (bands bent downward). Fast state density is not known for the etched surface but is 3×10^{11} cm^{-2} eV^{-1} for the oxidized surface. The S values of 10^3 to 3×10^4 agree

reasonably well with values for oxidized surfaces reported by Rosier[17] but not with the 5 to 10 cm per second values reported by Grove and Fitzgerald.[18] However, approximate agreement with the Grove and Fitzgerald values is obtained for an oxide which has been through boron and phosphorus diffusions, as discussed in Section 4.2.

Oxidation can thus provide satisfactory efficiency, but there are two rather serious objections to oxidation for this application:

(*i*) The oxidation must be done after the target is otherwise complete, and at this stage it frequently causes an increase in diode leakage current.

(*ii*) Vacuum bake-out of the tube and target at 350°C, which is desirable for good tube processing, may increase the interface state density and the recombination velocity.

Although both of these problems could be overcome by improved control of the oxide, an alternative procedure was found which obviated the final oxidation step for low S. Figure 7 shows the improvement in efficiency caused by a phosphorus diffusion on the light-receiving surface of a 4-mil thick target (circles). The phosphorus was diffused at 925°C for 10 min in PBr_3 vapor, yielding a depth of about 0.4 μ. This reduced S to a nominal value of 50 cm per second and the diffusion length was increased to 52 μ, yielding an efficiency of about 20 percent. The efficiency has been 50 to 60 percent on 1-mil thick targets.

Equation (8) is rather insensitive to surface-recombination velocity for $S \leqq 200$ cm per second, and 50 cm per second is only given as an approximate value. The phosphorus data in Fig. 7 were obtained with the phosphate glass on the surface. Removal of the glass did not change the response. When the diffused phosphorus layer was removed, the efficiency dropped to the original level for an etched surface, except for an upward displacement at long wavelengths resulting from the improved bulk lifetime. In some cases L_p has been increased to 100 μ ($\tau = 10$ μsec). The effect on S is evidently due to the built-in field of the diffused phosphorus layer which repels holes from the surface and causes a low recombination velocity. The principle of surface doping to reduce S was proposed by Moore and Webster[19] but we are not aware that a demonstration of it has been published. The slight droop in the phosphorus curve at about 0.5 μ, requiring a "dead layer" correction of 0.1 μ, seems to result from diffusion damage. At present the best conditions that have been found to minimize this effect are 850°C for 30 minutes.

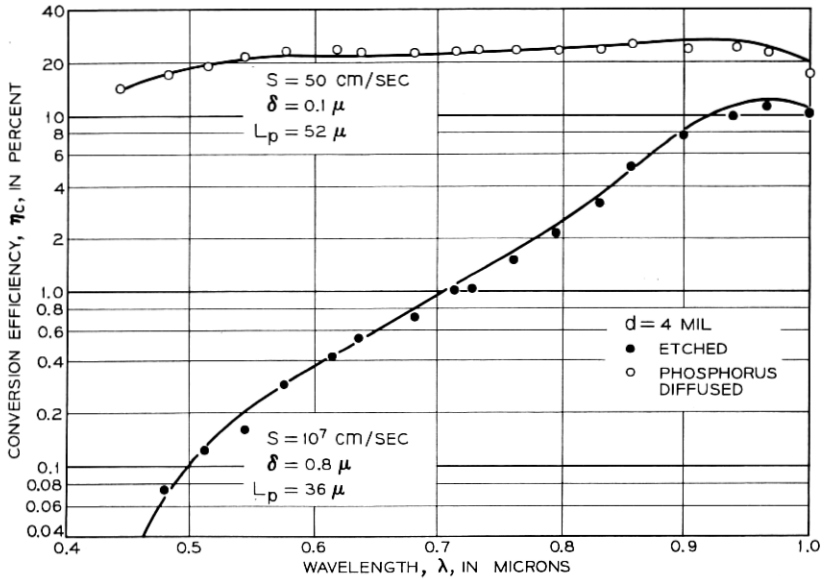

Fig. 7 — Effect of phosphorus diffusion on efficiency. Lower curve shows condition with etched surface before diffusion.

These results were all obtained on targets with large diodes, outside the tube. Results for a silicon target in a tube are shown in Fig. 8 where it is compared with a standard vidicon, and with the ideal case of unity conversion efficiency. Efficiency is expressed in units commonly used for vidicons, microamps of output current per microwatt of incident radiation. The curve for unity efficiency slopes upward because at longer wavelengths there are more photons per second per microwatt of radiation, with each photon capable of exciting an electron-hole pair. Efficiency of the silicon target is more than twice that of the vidicon in the middle of the visible region, and the sensitive range is much broader. The conversion efficiency exceeds 50 percent at a wavelength of 0.7 μ.

The diffused layer of phosphorus provides a very stable reduction in S which is unaffected by vacuum bake-out or deposition of antireflection coatings. Furthermore, the phosphorus treatment does not harm the diode characteristics; instead, it improves them as discussed in the next section. The phosphate glass must be removed from the p-type islands by a brief etch, but this requires no remasking.

IV. DARK CURRENT

4.1 *Bulk and Surface Generated Current*

Low dark current is another important requirement for this target. Current, in the absence of illumination, should not exceed 1×10^{-13} A per diode at 5 to 10 V reverse bias, or about 50×10^{-9} A for the whole array. Currents slightly above this range reduce the dynamic range of the camera tube or the available picture contrast. Currents five times greater prevent integration of the incident light flux over a full television scan period. The most readily observable effect of excessive dark current (more than 100×10^{-9} A) is "whiting out" of the picture on the display tube.

The dark current required for good performance is considerably lower than for most silicon devices. The reverse current in a target array can be separated into the two general categories of bulk generated current and surface generated current. An estimate of the bulk current can be obtained from the expression by Sah, Noyce, and Shockley[20] for current generated in the space-charge region:

$$I = qAwn_i\left\{2(\tau_p\tau_n)^{\frac{1}{2}} \cosh\left[\frac{E_t - E_i}{kT} + \tfrac{1}{2}\ln\left(\frac{\tau_p}{\tau_n}\right)\right]\right\}^{-1}. \qquad (10)$$

In equation (10) w is the depletion width, n_i the intrinsic carrier concentration, τ_p and τ_n the hole and electron minority carrier lifetimes on their respective sides of the junction and $E_t - E_i$ the energy dif-

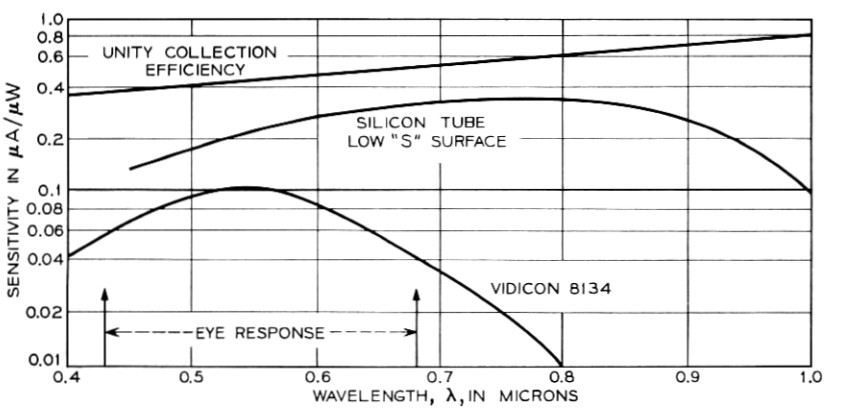

Fig. 8 — Comparison of 1 mil silicon target with antimony trisulfide target.

ference between an assumed single recombination-generation level and the intrinsic Fermi level. For an 8 μ diode at 10 V bias with the common simplifying assignment of $E_t = E_i$ and $\tau_p = 0.1$ μsec $> \tau_n$ as lifetime values representative of diffused structures, the current would be predicted by equation (10) as approximately 3×10^{-12} A. Since this estimate of bulk current alone exceeds the permissible dark current, diode leakage current was regarded as a potential source of difficulty for this device.

Of several diffusion conditions tried, those which yielded the lowest bulk generated reverse currents were 1140°C for 20 minutes with a BBr_3 source. These conditions gave a sheet resistance of 5 to 6 ohms per square and a junction depth of 2 μ. A subsequent phosphorus diffusion, which is required for ohmic contact and low S on the light-receiving surface, is an important part of the process. As a result of this treatment, the diffusion length was typically improved by a factor of three, while the reverse current, as measured on the 5-mil test diodes on the actual targets, was reduced by an order of magnitude to a median value of 10^{-12} A. In addition, the exponent in $I \propto V^n$ was reduced from $\sim$1.0 to $\sim$0.5.

The improvement in both the diffusion length and dark current by the phosphorus diffusion is presumably caused by a gettering action by the phosphate glass on impurities, such as gold and copper. A gettering effect has been suggested in several reports in which phosphorus treatments have improved silicon diode reverse characteristics[21-23] or minority carrier lifetime.[24, 25] The improvements in reverse current already described are quite similar to those reported by Ing and his coworkers about p^+n diodes of 0.9Ω-cm material.[22] In our work, neutron-activation analysis showed that a boron diffusion increased the gold concentration from approximately 4×10^{12} cm^{-3} to about 2×10^{13} cm^{-3}, while the phosphorus diffusion reduced it again to 4×10^{12} cm^{-3}. Insufficient sensitivity obscured any similar effect on copper if it was present. Cleaning the substrate with nitric acid or aqua regia before diffusion gave better post-boron I–V characteristics than did cleaning treatments without a strong oxidizing acid. The phosphorus treatment then caused further improvement.

The above process was developed using as control information the results of efficiency and dark current measurements on 5-mil test diodes available on target arrays, and also on the graduated-diameter diodes shown in Fig. 3. In addition to their function as control specimens, the graduated-diameter diodes were used to establish the rela-

tive importance of bulk and surface currents. This designation is made by assuming the total current to be a linear combination of an area and perimeter component:

$$I_r = I_{\mathcal{A}} + I_{\mathcal{P}} = \mathcal{A}D^2 + \mathcal{P}D, \tag{11}$$

where D is the diode diameter. It was possible to estimate $\mathcal{A}$ and $\mathcal{P}$ graphically from a plot of I_r/D vs D for the diodes of graduated diameter, and then calculate the $I_{\mathcal{A}}$ and $I_{\mathcal{P}}$ components for a diode of a particular diameter. In a typical case for a 5 mil diode, $I_{\mathcal{A}}$ was 4×10^{-13} A and $I_{\mathcal{P}}$ was 8×10^{-13} A. This corresponds to a bulk current density of 3.15×10^{-9} A per cm^2, and a perimeter current density of 2×10^{-11} A per cm. The relative importance of $I_{\mathcal{P}}$ becomes greater as the diode size decreases. Extrapolating to an 8 μ diode, $I_{\mathcal{A}} = 1.5 \times 10^{-15}$ A and $I_{\mathcal{P}} = 5 \times 10^{-14}$ A. Total dark currents of targets in tubes have been 5 to 50 $\times 10^{-9}$ A at 5 to 10 V or 2 to 20 $\times 10^{-14}$ A per diode, thus falling closer to the perimeter dependent limit.

The larger area diodes, which minimize the contribution of the surface current, permit assignment of $E_t - E_i$ in equation (10). In Fig. 9 the I–V characteristic of a typical 25 mil diode is shown with curves predicted by the Sah-Noyce-Shockley theory for different values of $E_t - E_i$. The reverse current density at 10 V for this diode was 6×10^{-9} A per cm^2. The lifetime τ_p of 5 μsec was obtained from conversion efficiency measurements. Also, τ_p was taken as much greater than τ_n and the argument of the cosh was greater than unity. The depletion-region width in equation (10) was obtained from experimental capacitance-voltage data and the expression $w = \epsilon A/C$. It may be seen in Fig. 9 that the reverse current calculated for the given 5 μsec lifetime and the single recombination center at about an $E_t - E_i$ of 0.08 to 0.1 eV matches the experimental I–V characteristic.

A quantity called the effective lifetime τ_{eff}, which is the lifetime obtained from equation (10) on the assumptions that $E_t = E_i$ and $\tau_{\text{eff}} = \tau_p = \tau_n$, may be used as a figure of merit to compare low leakage diodes of different resistivities. For our diodes, typical values of $\tau_{\text{eff}} = 100$ μsec were obtained. Ing and his co-workers obtained τ_{eff} between 10 and 40 μsec for their gettered diodes just described,[22] and Sah cited a τ_{eff} of 28 μsec for a high lifetime diode.[26]

Other measurements on our large area diodes also suggest the reverse current is dominated by bulk generation current within the space-charge region. Inversion layer surface leakage is not observed

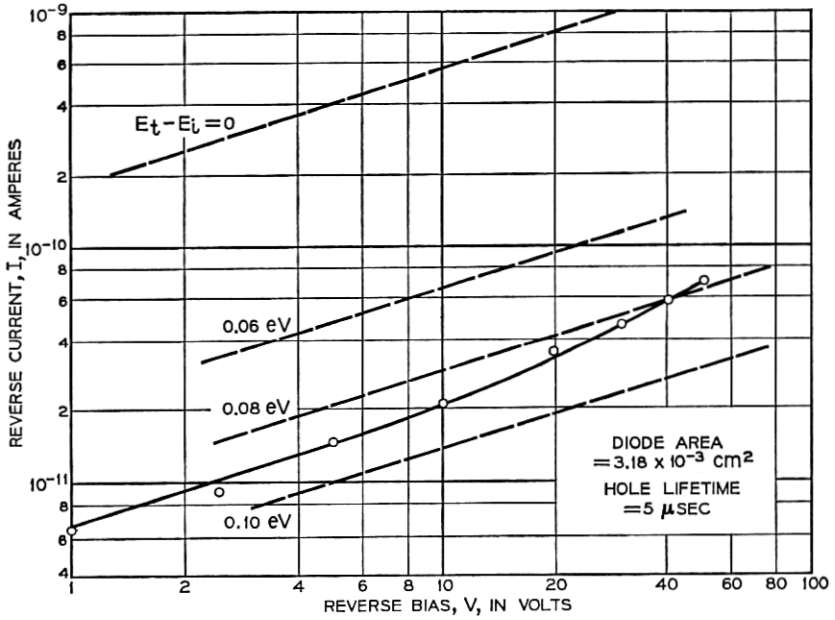

Fig. 9 — Reverse characteristic of 25 mil diode (circles) compared with characteristics predicted by Sah-Noyce-Shockley theory for different energy levels of recombination centers (dashed lines).

in these diodes, nor is it expected, since charge at the interface is positive and induces an n-type accumulation layer. The activation energy of reverse leakage current has been measured as 0.5 to 0.6 eV in the range 0 to 30°C. Such an activation energy is compatible with recombination-generation current rather than inversion layer (channel) leakage or with bulk diffusion current.[27] In addition, the forward I–V measurements are characterized by $1 < m < 1.3$ in the expression $I = I_o \exp(qV/mkT)$. Sah has found such a value of m for recombination-generation current.[26]

The foregoing observations were on relatively *large* diodes measured with no field applied across the passivating oxide. These results are all reasonably consistent with a model of reverse leakage current dominated by generation in the space-charge region of the metallurgical junction, and the currents are satisfactorily low when proper diffusion conditions are used.

4.2 *Leakage Induced by Electron-Beam Charging of the Oxide*

The satisfactory behavior observed for large diodes is a necessary condition if good arrays of small diodes are to be obtained. How-

ever, it may not be sufficient if the field induced by electron beam charging of the oxide leads to high surface-generated currents. In fact, the reverse characteristics of 8 μ diodes in target arrays, with a field across the oxide, are more complicated, although currents are still low enough at 5 to 7 V.

This section shows how surface generation current is influenced by a field across the oxide on the junction side of the array. At present, the problem of achieving low dark current in silicon target arrays is to reduce this type of leakage current. However, if improvement ten times better than present results is achieved, bulk generated reverse current will again become a problem.

The electron beam charging of the oxide can be simulated outside the tube by evaporating gold dots over both the oxide and p-regions and applying a negative bias. This gold dot structure then represents, in most respects, the situation in the camera tube, where the electron beam falls on both the diodes and the oxide. In Fig. 10 the experimental I–V curves are compared with the maximum allowable current of 50×10^{-9} A and the characteristic obtained for bulk generated current only. The bulk generated current curve is based on the assumption that the entire 1×10^{-12} A of reverse current for a 5-mil test diode is bulk current.

The top curve (data points given by $\triangle$) of Fig. 10 is a reverse characteristic measured by applying a negative bias to a 25-mil gold dot which covered 790 of the 8 μ diodes in a test array as illustrated in Fig. 2. The current was scaled up to 435,600 diodes.

The curve shown by the circles is a dark current characteristic measured in a tube. This curve shows behavior similar to the gold dot characteristic. However, the tube characteristics sometimes do not flatten out, for reasons not yet fully understood, although a few leaky diodes in the array are responsible in some cases. It may be seen that for these two curves the current rises steeply with increasing voltage and then changes slope abruptly between 6 and 10 V. Following the model of Grove and Fitzgerald,[18] this behavior can be described as current generated by interface states. This current increases, and finally saturates as a depletion layer is induced under the oxide. In specimens with resistivity more than about 8 Ω-cm, this depletion layer may result from the merging under the oxide of the space-charge regions of the 8 μ diodes, which are less than 12 μ apart edge to edge.

However, curves like those of Fig. 10 are also observed on targets with substrate resistivity as low as 0.1Ω-cm. In this case, the deple-

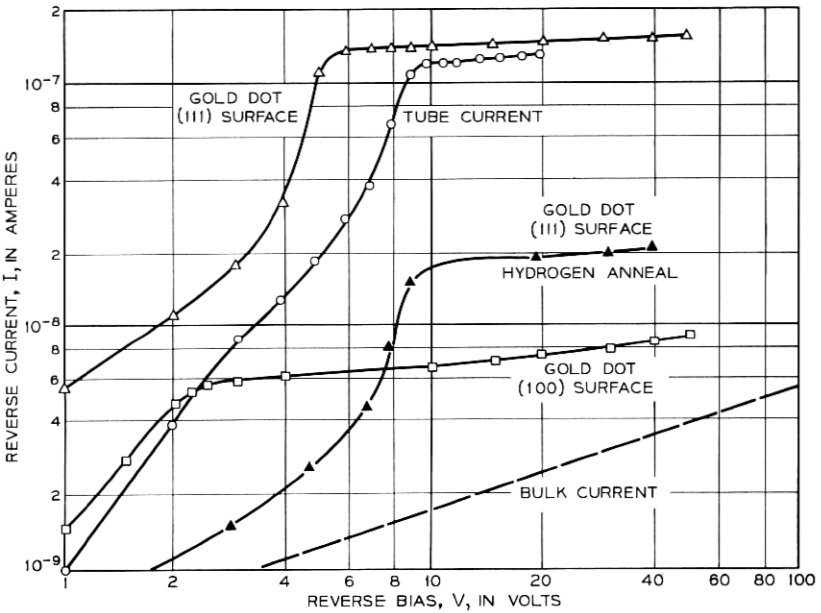

Fig. 10 — Total diode reverse current as a function of bias for target arrays. Current measured by contacting gold dots over diodes and oxide or as dark current in tube. Gold dot measurements cover 790 diodes and are extrapolated to 435,600 diodes. Dashed line would result from bulk space-charge generation alone. 5×10^{-8} amperes is the approximate upper limit for good performance.

tion is induced by a field normal to the semiconductor surface resulting from the negative bias on the gold dot, as in the gate controlled diodes of Grove and Fitzgerald.[18] In either case, the entire silicon surface between diodes is in a depleted condition. Every surface recombination-generation center on that part of the target surface not actually occupied by a diode contributes to the reverse current.

After depletion is established, the subsequent slower increase in reverse current beyond the discontinuity in Fig. 10 is caused by deepening of the space-charge regions under the oxide and around the metallurgical junctions. No decrease in current occurs at higher voltage across the oxide, as observed by Grove and Fitzgerald,[18] since in our case the potential on the oxide equals that on the p-region. Under these circumstances, inversion cannot occur to isolate the surface states from the depletion region.[18] Grove and Fitzgerald relate surface generation current to the surface-recombination velocity s_0 by the equation:

$$I = qn_i s_0 . \tag{12}$$

Using the current at the discontinuity s_o is estimated as 24 cm per second.

The density D_{ss} and electron capture cross section σ_s of interface states on a similar oxide, which had been through the same diffusion process, were measured by the MIS conductance technique of Nicollian and Goetzberger.[28] D_{ss} was 10^{11} cm^{-2} eV^{-1} near the center of the energy gap and σ_s was 2×10^{-16} cm^2. Using Grove and Fitzgerald's[18] definition of surface-recombination velocity for a depleted surface:

$$s_0 = \sigma s v_{th} \pi k T D_{ss} , \tag{13}$$

s_o is 16 cm per second with v_{th} as 10^7 cm per second. This value is in reasonable agreement with the value obtained from the generation current. In addition, conversion-efficiency measurements on a similar oxide, that is, one exposed to diffusion conditions, yielded surface-recombination values of about 50 cm per second. Notice, however, that the diode leakage and efficiency pertain to different values of surface potential.

The current at the discontinuity in gold dot I–V curves has been reduced by two methods. The upper curve in Fig. 10 for a (111) surface can be lowered to the solid triangle curve by hydrogen annealing at 500°C. The decrease in current by an order of magnitude at the discontinuity is assumed to result from a reduction in fast state density expected from this treatment.[29–31] A (100) silicon surface without hydrogen anneal produced the curve shown by squares. The current at the discontinuity has been lowered to 5.5×10^{-9} A at 2.5 V, presumably because of a reduction in interface state density.[29, 32] This current corresponds to an s_o of 1.6 cm per second. Thus, significant decreases in the leakage current have been made by these simple changes in processing and further improvement can reasonably be expected.

V. DEFECTS

A third very important requirement of any camera-tube target is freedom from defects. For the silicon target this means near perfection in an array of nearly ½ million diodes and the demands on planar technology are obviously severe. Leaky diodes, for example, can cause bright spot defects, while diodes which are covered and cannot be contacted by the electron beam, cause dark spot defects. Pinholes in the passivating oxide may cause bright spots by allowing the electron beam to contact the substrate directly. Certain dark

features have been identified with dislocation arrays revealed by etch pits in a neighboring slice of the crystal.

Not all defects can be explained at present. Figure 11 shows some which have been identified. They were intentionally introduced during the target processing. The picture at the top was taken with the camera tube viewing a transparency illuminated by tungsten light. Below it are photomicrographs taken of small areas of the target after it was removed from the tube. The dark area in the display corresponds to a spot in the array where oxide holes are missing because high spots in the oxide lifted the mask and allowed exposure of the photoresist over that area. The bright spot on the left corresponds to a large hole, revealed in the photomicrographs, which was etched in the oxide because contamination on the mask prevented exposure of the photoresist and, therefore, a hole was etched in the oxide. Boron diffused into that entire area and produced a large leaky diode. In ad-

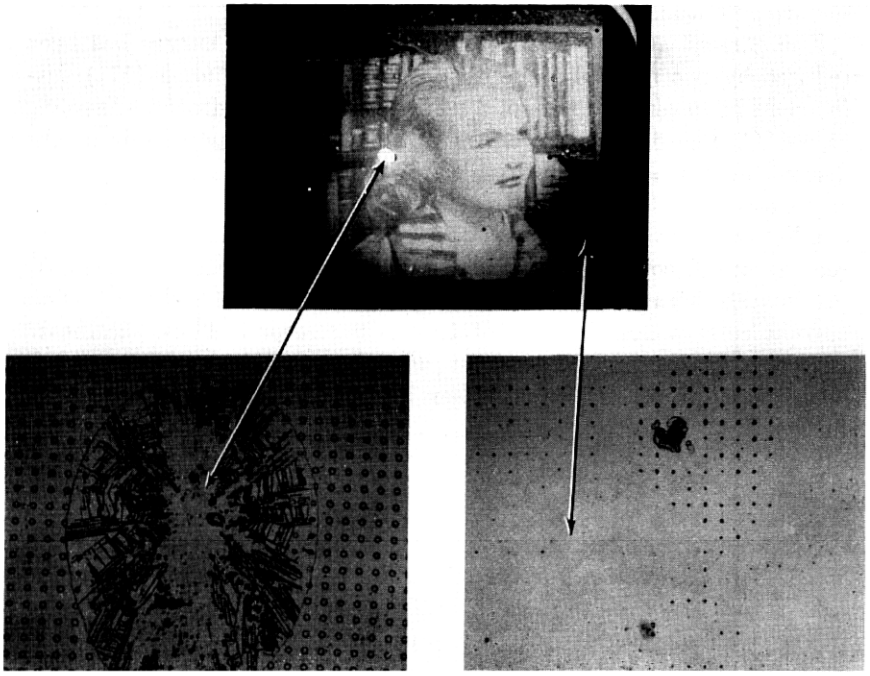

Fig. 11 — Example of gross defects in target. Top: picture from TV monitor. Lower right: photomicrograph of target showing spot where oxide holes are missing, corresponding to dark spot in display. Lower left: photomicrograph showing large hole in oxide which corresponds to bright spot in picture.

Fig. 12 — Picture taken with relatively defect-free target.

dition to defects associated with planar technology steps of target fabrication, bright spots can also be introduced by the deposition of the semi-insulating film for dissipating charge from the area between diodes.

The defects of Fig. 11 were introduced deliberately. Figure 12 shows a picture with only a few small, unintentional, defects visible. We have not yet made a target entirely free of defects. Substantially greater improvement in the defect situation has been made by the group at Bell Telephone Laboratories, Reading, Pa.[33]

VI. SUMMARY AND CONCLUSIONS

The status of the three important factors efficiency, diode leakage current, and defects in the array may be summarized as follows.

(*i*) Satisfactory conversion efficiency has been achieved. Surface recombination velocity (S) at the illuminated surface is the dominant

parameter controlling efficiency, and it should be $\leqq 10^3$ cm per second. Sufficiently low S can be obtained by wet chemical treatments or by oxidation in steam, but the most reliable treatment has been a phosphorus diffusion. This provides a built-in field which repels minority holes from the surface. S values of ≈ 50 cm per second, and efficiency of 40 to 60 percent throughout the visible region, have been obtained with this treatment. Adequate diffusion length, 30 to 100 μ (τ = 1 to 10 μsec) has also been obtained.

(*ii*) Diode leakage current is low enough ($\leqq 1 \times 10^{-13}$ A per diode or $\leqq 50 \times 10^{-9}$ A total dark current) for satisfactory operation at low target voltage ($\leqq 7$ V). Bulk generated current of $< 1 \times 10^{-8}$ A per cm^2 at 10 V is observed in large diodes (5 to 40 mil diameter). This would yield 4×10^{-15} A for an 8 μ diode. However, surface generation complicates the behavior when a field is applied across the passivating oxide as under a gold dot or in electron beam scanning. This causes an initial steep rise in current followed, usually, by an abrupt decrease in slope at 6 to 10 V. The current at which this occurs has been lowered substantially by use of (100) instead of (111) silicon slices and by hydrogen annealing.

(*iii*) Present technology produces targets which are reasonably defect-free but processing must be improved to eliminate defects completely. Leaky diodes or groups of diodes and oxide pinholes cause bright spots, while diodes which are covered and cannot be contacted by the electron beam cause dark spots. A decrease in average dark current should reduce the ability to observe fluctuations from diode to diode.

The emphasis on these three factors is not intended to imply that they are the only critical problems. Two others, discharging of the passivating oxide and resolution, have been studied by Crowell and Labuda.[2]

ACKNOWLEDGMENTS

We are indebted to R. H. Kaiser for taking the efficiency data, to R. Lieberman for help in studies of chemical processing and defects, to E. H. Nicollian for MOS conductance measurements, and M. H. Crowell and E. F. Labuda for useful discussions and data from their studies of tube behavior. We also wish to acknowledge the helpful interest of E. I. Gordon throughout the program.

REFERENCES

1. Crowell, M. H., Buck, T. M., Labuda, E. F., Dalton, J. V., and Walsh, E. J., "A Camera Tube with a Silicon Diode Array Target," B.S.T.J. *46,* No. 4 (February 1967), pp. 491–495.
2. Crowell, M. H. and Labuda, E. F., unpublished work.
3. Gordon, E. I., "A 'Solid-State' Electron Tube for the *PICTUREPHONE*® Set," Bell Laboratories Record *45,* No. 6 (June 1967), pp. 174–180.
4. Reynolds, F. W., "Solid State Light Sensitive Storage Device," U. S. Patent 3,011,089, issued November 28, 1961.
5. Heijne, L., "Photoconductive Properties of Lead-Oxide Layers," Philips Res. Rep. Supplement No. 4 (1961), pp. 149–154.
6. Wendland, P. H., "A Charge-Storage Diode Vidicon Camera Tube," IEEE Trans. Elect. Devices *ED-14,* No. 6 (June 1967), pp. 285–291.
7. Weimer, P. K., Forgue, J. V., and Goodrich, R. R., "The Vidicon Photoconductive Camera Tube," Electronics *23,* (May 1950), pp. 70–73.
8. van Roosbroeck, W., "The Transport of Added Current Carriers in a Homogeneous Semiconductor," Phys. Rev. *91,* (July 1953), pp. 282–289.
9. Wittry, D. B. and Kyser, D. F., "Measurement of Diffusion Lengths in Direct-Gap Semiconductors by Electron-Beam Excitation," J. Appl. Phys. *38,* No. 1 (January 1967), pp. 375–382.
10. Wittry, D. B. and Kyser, D. F., "Surface Recombination Velocities and Diffusion Lengths in GaAs," Proc. International Conf. on Physics of Semiconductors, Kyoto, 1966; J. Phys. Soc. Japan *21* Suppl., 1966, pp. 312–316.
11. Dash, W. C. and Newman, R., "Intrinsic Optical Absorption in Single-Crystal Germanium and Silicon at 77°K and 300°K," Phys. Rev. *99,* No. 4 (August 15, 1955), pp. 1151–1155.
12. Philipp, H. R. P., and Taft, E. A., "Optical Constants of Silicon in the Region 1 to 10 eV," Phys. Rev. *120,* No. 1 (October 1960), pp. 37–38.
13. Marquardt, D. W., "An Algorithm for Least-Squares Estimation of Nonlinear Parameters," J. Soc. Industrial Appl. Math. *11,* No. 2 (June 1968), pp. 431–441. The implementation of Marquardt's method used in this work is embodied in a program written by W. A. Burnette and C. S. Roberts of Bell Telephone Laboratories.
14. Buck, T. M. and McKim, F. S., "Effects of Certain Chemical Treatments and Ambient Atmospheres on Surface Properties of Silicon," J. Electrochem. Soc. *105,* No. 12 (December 1958), pp. 709–714.
15. Harten, H. U., "Surface Recombination of Silicon," Philips Res. Rep. *14,* (August 1959), pp. 346–360.
16. Many, A., Goldstein, Y., and Grover, N. B., *Semiconductor Surfaces* Amsterdam: North Holland Publishing Co., 1965, p. 138.
17. Rosier, L. L., "Surface State and Surface Recombination Velocity Characteristics of Si-SiO_2 Interfaces," IEEE Trans. Elec. Devices, *Ed-13,* No. 2 (February 1966), pp. 260–268.
18. Grove, A. S. and Fitzgerald, D. J., "Surface Effects on p-n Junctions: Characteristics of Surface Space-Charge Regions Under Non-Equilibrium Conditions" Solid-State Elec., *9,* No. 8 (August 1966), pp. 783–806.
19. Moore, A. R. and Webster, W. M., "The Effective Surface Recombination of a Germanium Surface with a Floating Barrier," Proc. I.R.E. *43,* No. 4 (April 1955), pp. 427–435.
20. Sah, C. T., Noyce, R. H. and Shockley, W. "Carrier Generation and Recombination in P-N Junctions and P-N Junction Characteristics," Proc. I.R.E. *45,* No. 9 (September 1957), pp. 1228–1243.
21. Goetzberger, A. and Shockley, W., "Metal Precipitates in Silicon P-N Junctions," J. Appl. Phys. *31,* No. 10 (October 1960), pp. 1821–1824.
22. Ing. S. W., Morrison, R. E., Alt, L. L., and Aldrich, R. W., "Gettering of Metallic Impurities from Planar Silicon Diodes," J. Electrochem. Soc. *110,* No. 6 (June 1963), pp. 533–537.

23. Lawrence, J. E., "Metallographic Analysis of Gettered Silicon," presented at AIME Conf. on Preparation and Properties of Elec. Materials, New York, August 28–30, 1967.
24. Waldner, M. and Sivo, L., "Lifetime Preservation in Diffused Silicon," J. Electrochem. Soc. *107,* No. 4 (April 1960), pp. 298–301.
25. Murray, L. A. and Kressel, H., "Improvement of Minority Carrier Lifetime in Silicon Diodes," Electrochem. Technology, *5,* No. 7–8 (July-August 1967), pp. 406–407.
26. Sah, C. T., "Effect of Surface Recombination and Channel on P-N Junction and Transistor Characteristics," IRE Trans. Elec. Devices, *ED-9,* (January 1962), pp. 94–107.
27. Bergh, A. A. and Bartholomew, C. Y., Jr., "The Effect of Heat Treatments on Low Current Gain with Various Ambients and Contamination," Late News Paper presented at Electrochem. Soc. Meeting, Philadelphia, Pa., October 14, 1966.
28. Nicollian, E. H. and Goetzberger, A., "The Si-SiO_2 Interface—Electrical Properties as Determined by the Metal-Insulator-Silicon Conductance Technique," B.S.T.J. *46,* No. 6 (July-August 1967), pp. 1055–1133.
29. Hofstein, S. R., "Stabilization of MOS Devices," Solid-State Elec., *10,* No. 7 (July 1967), pp. 657–670.
30. Balk, P., "Effects of Hydrogen Annealing on Silicon Surfaces," Extended Abstr., Electrochem. Soc. Meeting, May 9–13, 1965, pp. 237–240.
31. Schmidt, R., unpublished work.
32. Gray, P. V. and Brown, D. M., "Density of SiO_2-Si Interface States," Appl. Phys. Letters *8,* No. 2 (January 1966), pp. 31–33.
33. Batdorf, R. L., Beadle, W. E., Mathews, J. R., unpublished work.